ARTICLES

Microscopic annealing process and its impact on superconductivity in T'-structure electron-doped copper oxides

HYE JUNG KANG[1,2,3]*, PENGCHENG DAI[1,4]*, BRANTON J. CAMPBELL[5], PETER J. CHUPAS[6], STEPHAN ROSENKRANZ[6], PETER L. LEE[7], QINGZHEN HUANG[2], SHILIANG LI[1], SEIKI KOMIYA[8] AND YOICHI ANDO[8]

[1] Department of Physics and Astronomy, The University of Tennessee, Knoxville, Tennessee 37996-1200, USA
[2] NIST Center for Neutron Research, National Institute of Standards and Technology, Gaithersburg, Maryland 20899-8562, USA
[3] Department of Materials Science and Engineering, University of Maryland, College Park, Maryland 20742-2115, USA
[4] Neutron Scattering Sciences Division, Oak Ridge National Laboratory, Oak Ridge, Tennessee 37831-6393, USA
[5] Department of Physics and Astronomy, Brigham Young University, Provo, Utah 84602, USA
[6] Materials Science Division, Argonne National Laboratory, Argonne, Illinois 60439, USA
[7] Advanced Photon Source, Argonne National Laboratory, Argonne, Illinois 60439, USA
[8] Central Research Institute of Electric Power Industry, Komae, Tokyo 201-8511, Japan
*e-mail: hkang@nist.gov; daip@ornl.gov

High-transition-temperature superconductivity arises in copper oxides when holes or electrons are doped into the CuO_2 planes of their insulating parent compounds. Whereas hole doping quickly induces metallic behaviour and superconductivity in many cuprates, electron doping alone is insufficient in materials such as R_2CuO_4 (R is Nd, Pr, La, Ce and so on), where it is necessary to anneal an as-grown sample in a low-oxygen environment to remove a tiny amount of oxygen in order to induce superconductivity. Here we show that the microscopic process of oxygen reduction repairs Cu deficiencies in the as-grown materials and creates oxygen vacancies in the stoichiometric CuO_2 planes, effectively reducing disorder and providing itinerant carriers for superconductivity. The resolution of this long-standing materials issue suggests that the fundamental mechanism for superconductivity is the same for electron- and hole-doped copper oxides.

The parent compounds of the high-transition-temperature (high-T_c) copper-oxide superconductors are antiferromagnetic (AF) Mott insulators composed of two-dimensional CuO_2 planes separated by charge reservoir layers[1–3]. When holes are doped into these planes, the static long-range AF order is quickly destroyed and the lamellar copper-oxide materials become metallic and superconducting over a wide hole-doping range. In the case of electron-doped materials such as the T'-structured R_2CuO_4 (R is Nd, Pr, La, Ce and so on), electron doping alone is insufficient, and annealing the as-grown sample in a low-oxygen environment to remove a tiny amount of oxygen is necessary to induce superconductivity[2,3]. Previous work[4–23] suggests that oxygen reduction may influence mobile carrier concentrations[7], decrease disorder/impurity scattering[8,10,11,23] or suppress the long-range AF order[16,17,22]. However, the microscopic process of oxygen reduction and its effect on the large electron–hole phase-diagram asymmetry and the mechanism of superconductivity[2,3] are still unknown. Here we use X-ray and neutron-scattering data, combined with chemical and thermogravimetric analysis measurements, in the electron-doped $Pr_{0.88}LaCe_{0.12}CuO_4$ to show that the microscopic process of oxygen reduction is to repair Cu deficiencies in the as-grown

materials[12,13] and to create oxygen vacancies in the stoichiometric CuO_2 (refs 16,17,22), effectively repairing disorder in the CuO_2 planes and providing itinerant carriers for superconductivity.

The role of the reduction process in the superconductivity of electron-doped high-T_c copper oxides has been a long-standing unsolved problem. For the hole-doped cuprates, low doping levels (for example 5%) entirely suppress AF order and superconductivity appears over a wide range of hole concentrations (from 6 to 30%). In the case of T'-structured electron-doped superconductors, doping alone by substituting the trivalent ions R^{3+} in R_2CuO_4 with tetravalent Ce^{4+} is insufficient to induce superconductivity, and the as-grown materials such as $Nd_{2-x}Ce_xCuO_{4\pm\delta}$ (NCCO), $Pr_{2-x}Ce_xCuO_{4\pm\delta}$ (PCCO) and $Pr_{0.88}LaCe_{0.12}CuO_4$ (PLCCO) are semiconducting with static long-range AF order[4–22]. In these materials, superconductivity (maximum $T_c \sim 25$ K) is achieved only when the samples within a relatively narrow dopant range ($0.1 \leq x \leq 0.18$) are annealed in a reducing atmosphere[2–23]. The reduction process suppresses the AF order most severely at higher Ce-doping levels above $x \geq 0.1$ (ref. 14). This so-called 'materials issue' in T'-structured electron-doped superconductors raises the question of whether
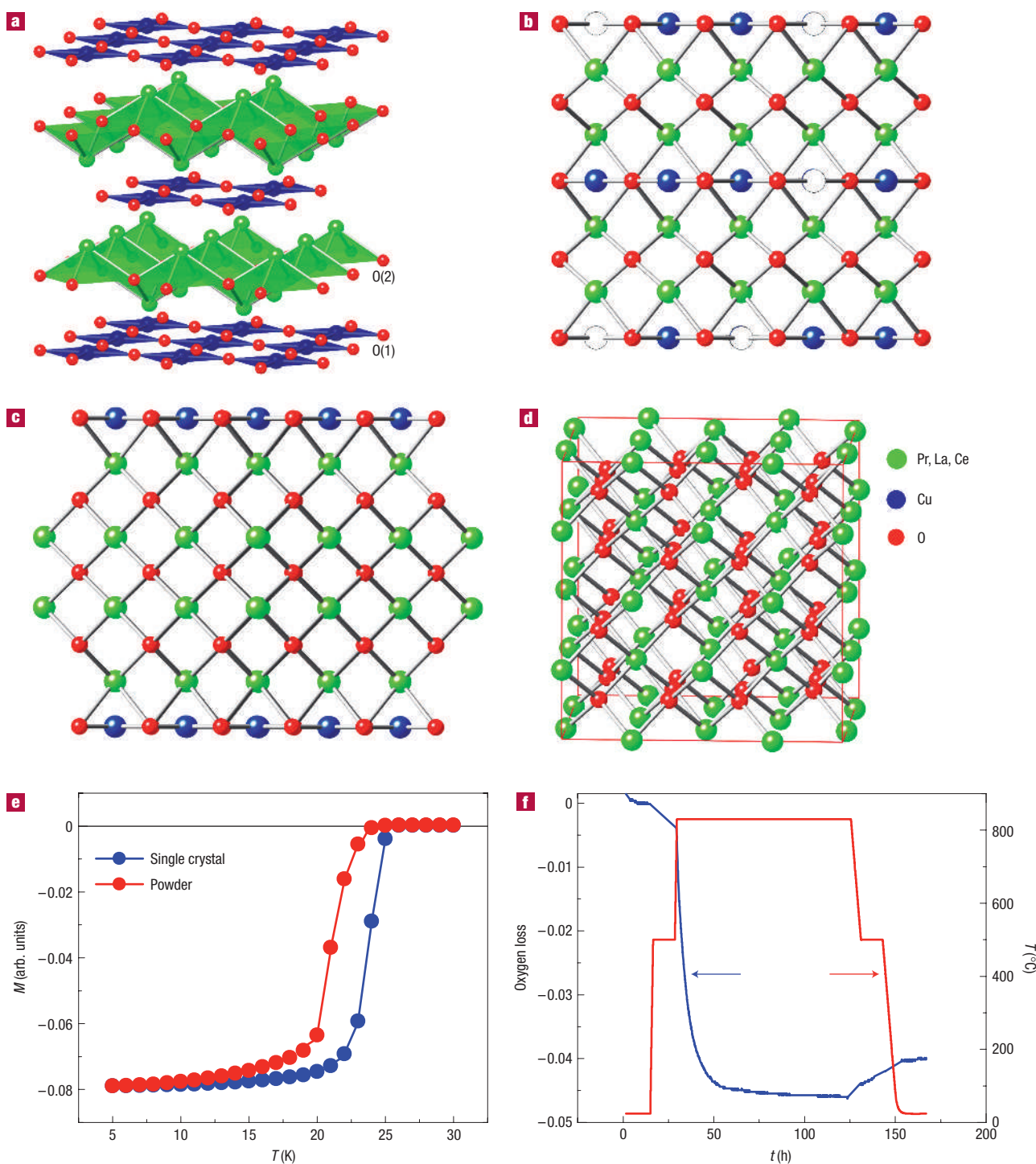
Figure 1 Crystal structures, magnetic susceptibilities and TGA measurements. a, Typical T' structure ($I4/mmm$) of PLCCO consisting of CuO_2 sheets separated by thin sheets of rare-earth oxide (Pr,La,Ce)O. **b**, T' structure of as-grown PLCCO with random Cu vacancies in the CuO_2 planes. **c**, A modified T' structure in which Cu atoms have been removed from one layer, leaving behind a thin slab of the anion-deficient fluorite impurity phase: $R_2O_3 = (Pr,La,Ce)_2O_3$. **d**, The vacancy-ordered C-type sesquioxide structure of the R_2O_3 impurity phase (space group $Ia3$). **e**, Magnetic susceptibilities of the r-SC single-crystal and ceramic powder samples as a function of temperature. **f**, Oxygen losses during the reduction process measured with a TGA. The mass change between 500 °C and room temperature is mainly due to the intrinsic properties of the TGA instrument in vacuum.

the fundamental mechanism for superconductivity is the same for electron- and hole-doped superconductors. For example, whereas the symmetry of the superconducting order parameter in

hole-doped superconductors is generally believed to be d wave[24], there has been no consensus on the nature of the superconducting order parameter in electron-doped materials[25]. A resolution of the
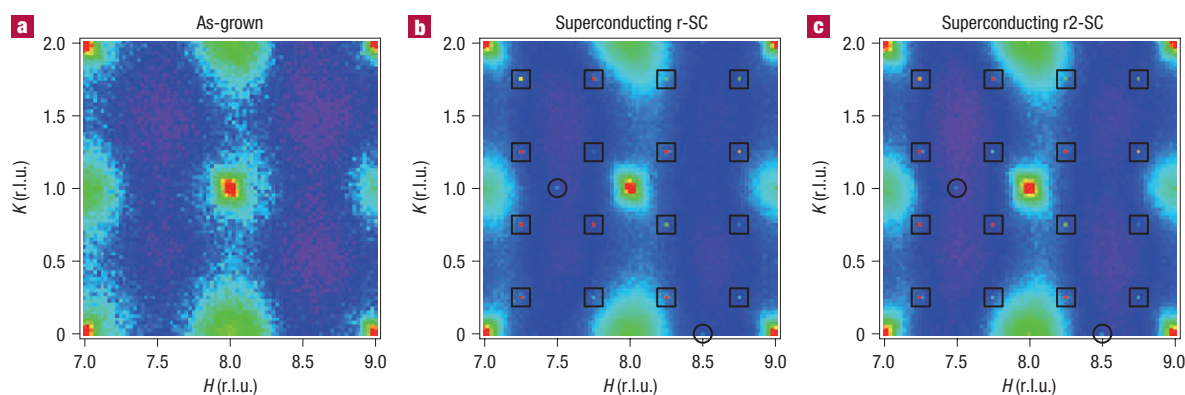
Figure 2 Single-crystal X-ray diffraction mesh scans in the (H, K) plane at $L = 1.1$. PLCCO samples show thermal diffuse scattering around intense Bragg reflections. **a**, The ag-NSC sample shows no evidence of the R_2O_3 impurity phase. **b**, The r-SC sample, prepared by reducing the ag-NSC sample, shows peaks at (1/2, 0) and (1/4, 1/4) positions (marked by squares and circles, respectively) associated with epitaxial intergrowths of the R_2O_3 impurity phase. **c**, The r2-SC sample shows identical behaviour to r-SC.

'materials issue' surrounding the annealing process should allow us to focus on the intrinsic similarities and differences between the electron- and hole-doped superconductors.

Originally, Tokura et al.[2,3] suggested that an as-grown sample had stoichiometric oxygen. The reduction process removes oxygen in the CuO_2 plane (making oxygen content less than 4), and therefore introduces mobile electrons into the system[2]. This microscopic oxygen-reduction mechanism was proposed on the basis of resistivity values from undoped Nd_2CuO_4 samples, which were found to decrease dramatically on quenching from $1{,}150\,^{\circ}C$ to room temperature. Although experiments using a thermogravimetric analyser (TGA) confirm that the reduction process removes some of the oxygen[4–6], this simple model is inconsistent with observations that as-grown samples have excess oxygen per Cu atom[7–9] and that superconductivity is not achieved at any Ce (that is, electron) doping levels without subsequent oxygen reduction.

Using neutron diffraction, resistivity and Hall-effect measurements, Greene and co-workers argue that the annealing process increases the number of mobile charge carriers[7] or decreases impurity scattering by removing apical oxygens (proposed oxygen just above and below the Cu atoms of the CuO_2 planes), which should be absent from the ideal T' structure of electron-doped materials[8,10,11,23]. In this latter model, the presence of a small amount of randomly doped apical oxygen in the as-grown materials induces localization of doped electrons and thus prohibits superconductivity. The role of the oxygen-reduction process would then be to remove the excess apical oxygen and increase the mobility of doped electrons to allow metallic behaviour and superconductivity[8,10,11,23].

Although the reduction process is widely believed to involve removal of the apical oxygen, such a notion has recently been challenged by Raman, infrared-transmission and ultrasound studies of electron-doped materials[16,17,22]. Instead of removing apical oxygen, these experiments on NCCO and PCCO suggest that the reduction process removes the oxygen in the CuO_2 plane (O(1), see Fig. 1a) at high Ce doping ($x \geq 0.1$) and the apical oxygen at low Ce doping[16,17]. In such a circumstance, the in-plane oxygen defect created by the reduction would be responsible for superconductivity by destroying the long-range antiferromagnetism and increasing the mobility of charge carriers[16,17,22]. Because the antiferromagnetism is much less affected

at low Ce doping levels[14], superconductivity is not achieved for $x < 0.1$ even though the samples are reduced.

Although these current microscopic scenarios seem plausible, they all miss a key ingredient of the problem; that is, none of these models can explain why the appearance of superconductivity after oxygen reduction is also intimately related to the creation of an epitaxially grown impurity phase of cubic R_2O_3 (refs 15, 18–21). Experimentally, it was found that about 1–2% of the impurity phase, absent from the as-grown materials, appears with superconducting phase after the oxygen-reduction process[18–21]. Although not explicitly demonstrated, the R_2O_3 impurity phase may disappear again when annealed samples are oxygenated to eliminate superconductivity[15,21]. Therefore, superconductivity in electron-doped materials might be intimately related to the appearance of the impurity phase.

Here we used systematic X-ray- and neutron-diffraction measurements, combined with chemical and TGA measurements in single crystals and powders of PLCCO, to elucidate the microscopic origin of the annealing process. Because of Cu evaporation during the high-temperature synthesis process, a small amount of Cu deficiency ($\sim$1%) was found in the stoichiometrically prepared as-grown NCCO[12,13]. According to Kang et al.[20], as-grown samples of PLCCO may also be Cu deficient. To test this possibility, single crystals of PLCCO (space group $I4/mmm$, $a = 3.98\,Å$, $c = 12.3\,Å$) were grown using the travelling-solvent floating-zone technique. These included four samples prepared from the same as-grown batch: as-grown non-superconducting (ag-NSC), reduced superconducting (r-SC), oxygenated non-superconducting (o-NSC) and re-reduced superconducting (r2-SC) crystals.

As shown in previous work[18–21], annealing necessary to produce superconductivity also induces epitaxial intergrowths of the cubic R_2O_3 impurity phase. The R_2O_3 has a cubic structure with space group $Ia3$ and lattice parameter $a_c = 2\sqrt{2}a \sim c/1.1$, where the 'c' subscript indicates 'cubic'. The Miller indices of the T' and impurity phases are related as $(H, K, L) = [(H_c - K_c)/4, (H_c + K_c)/4, L = 1.1L_c]$. Because the lattice parameter of R_2O_3 matches the in-plane lattice parameter of the T' phase but is $\sim$10% less than the c-axis lattice parameter of the T' phase, Bragg reflections from the impurity phase should occur at commensurate positions in the (H, K) reciprocal space plane but at $L = 1.1$, 2.2, and so on. For odd values of L, structure
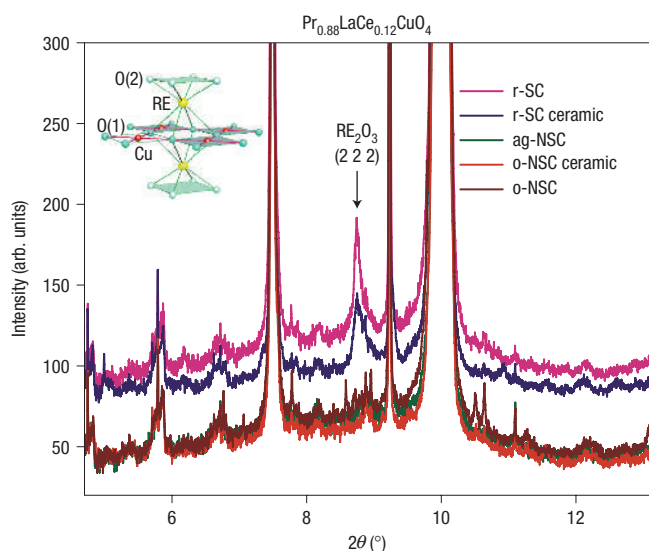
Figure 3 X-ray powder-diffraction patterns from crushed single-crystal and ceramic powder samples. The SC samples reveal the $(2,2,2)_c$ Bragg reflection of the R_2O_3 impurity phase at $2\theta = 8.7°$. The inset illustrates the T' crystal structure and atom labels used in Rietveld refinements.

factors of the impurity phase become non-zero at (1/2, 0) and (1/4, 1/4) type positions[18–21]. Figure 2 summarizes X-ray diffraction mesh scans of the (H, K) reciprocal space plane of PLCCO at $L = 1.1$ taken from the ag-NSC, r-SC and r2-SC single-crystal samples. The data from the ag-NSC (Fig. 2a) reveal fundamental Bragg peaks in the T' phase associated with thermal diffuse scattering. In the SC sample (Fig. 2b), a new set of peaks develops at (1/2, 0)- and (1/4, 1/4)-type positions, confirming the presence of the impurity phase.

To test the reversibility of the impurity phase, we carried out X-ray powder-diffraction measurements on portions of the ag-NSC, r-SC and o-NSC single-crystal samples of PLCCO that were crushed into fine powders. In addition, r-SC and o-NSC ceramic samples of PLCCO were prepared and analysed for comparison with the crushed single-crystal samples. Figure 3 shows a portion of the X-ray powder patterns from each of these samples. The two SC samples clearly reveal the $(2, 2, 2)_c$ reflection of the R_2O_3 impurity phase at $2\theta = 8.7°$. This peak is conspicuously absent from the three NSC samples. Furthermore, the impurity phase appears again in the re-reduced r2-SC single crystal (Fig. 2c). These results conclusively show that the impurity phase grows epitaxially parallel to the a–b plane of the T' cuprate structure, and it is reversibly

created on oxygen reduction to the SC state and destroyed on oxidation to the NSC state. Thus, the oxygen-reduction process is completely reversible and intimately related to the appearance of the impurity phase and superconductivity in PLCCO.

To understand this phenomenon, consider an annealing process that causes a slightly Cu-deficient T' material to phase separate into a Cu-perfect T' majority phase and a Cu-free minority phase. As shown in Fig. 1a–d, removing the Cu atoms from a single CuO_2 plane results in a locally primitive pseudo-cubic oxygen sublattice with 50% of the cubic interstices filled by rare-earth atoms. When viewed from the [1,1,0] direction, this structure cannot be distinguished from that of fluorite, though the rare-earth sublattice is not yet face centred. The creation of one oxygen vacancy for each Cu atom removed, followed by a vacancy-assisted one-interstice displacement of the nearby rare-earth atoms on one side of the affected sheet, then produces the familiar face-centred rare-earth sublattice of fluorite—a 25% anion-deficient fluorite in fact. This 25% anion vacancy concentration marks the extreme limit of stability for the fluorite structure and is only known to occur in the vacancy-ordered structure type commonly referred to as the 'C-type sesquioxide' or the 'bixbyite' structure. If we assume that ag-NSC samples are composed of $R_2Cu_{1-f}O_{4-\alpha}$, where f and α are Cu and oxygen deficiencies respectively, the annealing process can be written as $R_2Cu_{1-f}O_{4-\alpha} = (1-f)(R_2CuO_{4-\beta}) + f(R_2O_3) + (-\alpha + \beta + f(1-\beta))$ (O), where β is the oxygen deficiency level in the superconducting part of R_2CuO_4.

The appeal of such a structural reorganization lies in the fact that the observed R_2O_3 impurity phase has precisely the C-type sesquioxide structure. The Cu atoms removed from the affected sheet, rather than irreversibly leaving the sample, are free to fill vacancies in other layers, thus 'repairing' most of the Cu vacancies in the majority T' phase. Moreover, just as oxygen removal seems to drive the phase separation, subsequent high-temperature oxidation is assumed to drive a redistribution of Cu vacancies throughout the sample and the concomitant elimination of the epitaxial sheets of R_2O_3. Such an annealing process is entirely reversible, and benefits from the fact that the T' structure is stable against Cu deficiencies owing to the three-dimensionally interconnected rare-earth–oxygen network[5] that includes rather than being interrupted by CuO_2 planes.

To establish any Cu deficiencies in the samples, we carried out inductively coupled plasma (ICP) atomic-emission spectroscopy analysis on ag-NSC, an r-SC and o-NSC PLCCO crystals. Similar measurements were also carried out on ceramic PLCCO samples. The ICP results are summarized in Table 1 and indicate that all samples have a small Cu deficiency. It is worth noting here that the ICP analyses provide no information on oxygen content, and that they average over the T' cuprate and Cu-free impurity components of the mixed-phase SC samples. They should, therefore, be taken as a qualitative rather than a quantitative indicator of Cu deficiency.

Table 1 Nominal PLCCO metal compositions via ICP analysis. ICP standard solutions were prepared by dissolving Pr_6O_{11}, La_2O_3, CeO_2 and CuO powders in HNO_3. Each rare-earth powder was baked to remove moisture before measuring its mass. For each PLCCO sample, 30 mg of material was dissolved into 100 ml of HNO_3 (1 mol l^{-1}) acid. The compositions are normalized to give a Pr composition of 0.88.

Samples	Nominal composition from ICP measurement
ag-NSC	$Pr_{0.88}La_{0.95}Ce_{0.10}Cu_{0.90}$
r-SC	$Pr_{0.88}La_{0.95}Ce_{0.10}Cu_{0.90}$
o-NSC	$Pr_{0.88}La_{0.95}Ce_{0.10}Cu_{0.90}$
r-SC ceramic	$Pr_{0.88}La_{1.01}Ce_{0.10}Cu_{0.95}$

Table 2 Nominal PLCCO compositions and phase fractions from X-ray powder diffraction. The 1.6% volume fraction of the impurity phase in the SC samples is much more sensitive to X-rays than neutrons because of rare-earth atoms' relatively high X-ray scattering amplitude. This value is comparable to the difference in Cu deficiency levels between the NSC and SC samples.

Samples	Nominal composition from X-ray scattering	Volume fraction of $(Pr,La,Ce)_2O_3$
ag-NSC	$Pr_{0.88}LaCe_{0.12}Cu_{0.962(3)}O_4$	
o-NSC ceramic	$Pr_{0.88}LaCe_{0.12}Cu_{0.962(3)}O_4$	
o-NSC	$Pr_{0.88}LaCe_{0.12}Cu_{0.970(4)}O_4$	
r-SC	$Pr_{0.88}LaCe_{0.12}Cu_{0.983(4)}O_4$	0.0163 (1.63%)
r-SC ceramic	$Pr_{0.88}LaCe_{0.12}Cu_{0.990(4)}O_4$	0.0157 (1.57%)

To quantitatively determine the volume fraction of the impurity phase, we carried out the Rietveld analysis of the X-ray powder patterns using the GSAS software as summarized in Table 2. The volume fraction of the impurity phase in the SC samples is about 1.6%. The composition of PLCCO was also refined, yielding average Cu deficiencies of 3.5% in the NSC samples and 1.4% in the SC samples. The difference in Cu deficiency between the NSC and SC samples is then quite close to the refined volume fraction of the impurity phase (~1.6%), further confirming the relationship between Cu vacancies and impurity phase formation.

The use of an X-ray refinement to determine the absolute occupancy of each unique atom in PLCCO is difficult because of its coupling to the atomic displacement parameters (that is, thermal factors). To obtain better occupancies, neutron powder-diffraction data were collected using two different wavelengths, after which combined double-wavelength Rietveld refinements were carried out. The key results are summarized in Table 3; the most interesting of these are the differences in Cu and oxygen occupancies between the SC and the NSC samples. The occupancy of in-plane oxygen O(1) (Fig. 3 inset) is also significantly more deficient in the SC samples (~1%). The Cu occupancy is 1.2–2.3% deficient in the NSC samples, but recovers full occupancy in the SC samples. Once again, the difference in Cu-deficiency levels between SC and NSC samples is comparable to the volume fraction of the impurity phase obtained from X-ray scattering. Because the impurity phase does not contain Cu, the missing Cu in an NSC sample should be consistent with the volume fraction of the impurity phase in an SC sample. Furthermore, because the impurity phase forms via oxygen reduction as illustrated in Fig. 1, one should be able to predict the amounts of the oxygen loss using the results of Table 3 and compare them with actual TGA oxygen-loss measurements for each sample. This is indeed the case as shown in the Methods section.

Using the refinement results in Table 3, one can also normalize the Cu occupancies to one to obtain Cu:O ratios. The SC samples have normalized oxygen occupancies less than 4 in the chemical formula unit (for example $CuO_{4-\beta}$ with $\beta \approx 0.06$), whereas the NSC samples have normalized oxygen occupancies greater than 4 (for example $CuO_{4-\alpha}$ with $-\alpha \approx 0.02$–0.07). Based on these oxygen occupancies and bond lengths[26], we estimate the valence of Cu to be 1.66 for the SC samples and 1.72 in the NSC samples. The decrease of Cu valence in the SC samples indicates that the SC samples have slightly more doped electrons than the NSC samples. This is mainly due to a smaller number of oxygen atoms per Cu atom, because there is little difference in the bond lengths between the SC and the NSC samples. Although the annealing process only marginally affects the effective electron-doping level, it is large enough to increase electron mobility and decrease the resistivity in the annealed undoped samples[2].

The Cu deficiency in as-grown electron-doped materials provides a natural explanation of its electronic properties, effectively weakening the electron-doping effect of Ce by increasing numbers of oxygens and therefore adding holes per Cu atom. In the present model, the annealing process diminishes any Cu deficiency and therefore promotes the electron-doping effect of Ce, which also suppresses the AF Néel temperature (T_N). Our recent systematic neutron diffraction measurements on PLCCO as a function of annealing process showed that the T_N of PLCCO drops from 186 K in an ag-NSC sample to <600 mK in an r-SC sample ($T_c = 24$ K); refs 27,28.

From recent Hall-coefficient measurements, it has been argued[29] that the annealing process does not affect the carrier concentration but rather affects the mobility of the carriers. Because random Cu and oxygen vacancies in the CuO_2 plane break the translational symmetry of the CuO_2 plane, they can act as impurity centres to localize the doped electrons. The observed

Table 3 Neutron refinement results of PLCCO samples. All samples were refined in space group _I4/mmm_. Occupancies are shown in terms of atoms per chemical formula unit. The statistical deviations of refined parameters are included in parentheses. The principal difference between the SC and the NSC samples is a significantly lower Cu deficiency and a lower bond valence in the SC samples.

Parameter	r-SC	ag-NSC	r-SC ceramic	o-NSC ceramic
n (Pr)	0.88	0.88	0.88	0.88
n (La)	0.962(8)	0.978(8)	0.958(8)	0.960(8)
n (Ce)	0.12	0.12	0.12	0.12
z	0.35312(5)	0.35273(5)	0.35302(5)	0.35277(4)
$u_{11} = u_{22}$ ($Å^2$)	0.0056(2)	0.0051(2)	0.0053(2)	0.0049(2)
u_{33} ($Å^2$)	0.0084(4)	0.0078(4)	0.0072(3)	0.0070(3)
n (Cu)	1.001(6)	0.977(6)	1.001(6)	0.988(5)
$u_{11} = u_{22}$ ($Å^2$)	0.0056(3)	0.0051(3)	0.0064(3)	0.0063(2)
u_{33} ($Å^2$)	0.0129(5)	0.0106(5)	0.0109(4)	0.0100(4)
n (O(1))	1.95(1)	1.98(1)	1.94(1)	1.97(1)
u_{11} ($Å^2$)	0.0091(4)	0.0090(4)	0.0105(4)	0.0100(3)
u_{22} ($Å^2$)	0.0062(4)	0.0119(4)	0.0073(4)	0.0091(3)
u_{33} ($Å^2$)	0.0155(4)	0.0126(4)	0.0140(4)	0.0129(3)
n (O(2))	2.00	2.00	2.00	2.00
$u_{11} = u_{22}$ ($Å^2$)	0.0071(2)	0.0068(2)	0.0085(2)	0.0074(2)
u_{33} ($Å^2$)	0.0146(4)	0.0121(3)	0.0126(3)	0.0120(3)
Ratio(Cu:O)	**$CuO_{3.95}$**	**$CuO_{4.07}$**	**$CuO_{3.94}$**	**$CuO_{4.02}$**
RE-O(1) ($Å$)	2.6922(4)	2.6948(4)	2.6933(4)	2.6952(4)
RE-O(2) ($Å$)	2.3640(3)	2.3609(3)	2.3636(3)	2.3615(3)
O(1)-O(1) ($Å$)	2.81995(3)	2.81921(3)	2.82001(2)	2.81923(2)
O(1)-O(2) ($Å$)	3.07875(4)	3.07805(3)	3.07940(3)	3.07980(3)
Cu-O(1) ($Å$)	1.99401(2)	1.99348(2)	1.99405(1)	1.99350(2)
$R(F^2)$ (%)	5.6	6.2	4.5	4.1
wR (%)	5.4	5.4	5.9	5.62
χ^2	1.377	1.383	1.223	1.248
Cu bond valence (e.u.)	**1.66**	**1.73**	**1.66**	**1.71**

increase in charge carrier mobility would then seem to be the result of eliminating the Cu vacancies and repairing the CuO_2 planes of the T' structure. Of course, the creation of oxygen defects in the CuO_2 plane as a by-product of the oxygen-reduction process (Table 3) may also be necessary to suppress the AF order and increase the electron mobility[16,17,22], thereby facilitating superconductivity in the electron-doped cuprates.

Differences in the phase diagrams[2,3] and the electronic properties[24,25] of the electron- and hole-doped cuprate superconductors have been obscured by the 'materials issue' surrounding the annealing process in the electron-doped samples. The microscopic oxygen-reduction process presented here removes much of the mystery and will need to be taken into account to resolve any intrinsic differences between electron- and hole-doped superconductivity. Angle-resolved photoemission measurements on NCCO (ref. 30) and PLCCO (ref. 31) have recently determined the Fermi surface topology and the superconducting gap function in electron-doped materials. However, the quality of the sample surfaces studied has not been conclusively established, and the possible effect of an exposed NSC R_2O_3 surface must now be considered in future angle-resolved photoemission and scanning tunnelling microscopy experiments. Furthermore, it should also be possible to grow higher-quality single-crystal T'-structured copper oxides by adding excess Cu in the starting materials to eliminate Cu deficiencies and subsequent R_2O_3 contamination.

Because of the availability of single crystals of the T'-structured copper oxides, the vast majority of transport, structural, magnetic and electronic-property measurements of electron-doped superconductors have been obtained from these materials[9–22,25,27–31]. For other electron-doped high-T_c

superconductors with different crystal structure types, such as the infinite-layer $Sr_{1-x}La_xCuO_2$ family[32–34], the microscopic process of inducing superconductivity is still unclear[33,34]. There, the large single crystals that have made numerous single-crystal X-ray and neutron-scattering experiments possible in the T' materials[18–21] are not currently available. In the case of the T'-structured materials, however, we can return our focus to the electronic properties of the CuO_2 planes themselves in the search for a mechanism of superconductivity.

METHODS

Single crystals of PLCCO were grown using the travelling-solvent floating-zone technique. Four samples (ag-NSC, r-SC, o-NSC, and r2-SC) were then prepared from the same as-grown batch of crystals[27]. Single-crystal X-ray diffraction experiments were carried out at room temperature with 30 keV X-rays at the BESSRC 11-ID beamline of the Advanced Photon Source (APS) at Argonne National Laboratory. Synchrotron X-ray powder-diffraction measurements were made at a wavelength of 0.49582 Å on the 32-ID beamline at APS. Reciprocal lattice vectors have been defined relative to the T' cuprate lattice of PLCCO and are labelled as $(H, K, L) = (Q_x a, Q_y a, Q_z c)/2\pi$ reciprocal lattice units (r.l.u.), where $\mathbf{Q} = (Q_x, Q_y, Q_z)$ is the scattering wavevector in units of $Å^{-1}$. Rietveld refinements were carried out on powder-diffraction data to obtain site occupancies and phase fractions. Because the rare-earth atoms (Pr, La, Ce) share a single site and very similar X-ray scattering amplitudes, their relative ratios were fixed according to the nominal synthetic composition, and the total rare-earth occupancy was normalized to 2. Because of the weak relative X-ray-scattering amplitude of oxygen, the oxygen occupancies were also fixed at 100%. Thus, only the Cu occupancy and the impurity phase fraction were refined (Table 2).

Neutron-diffraction measurements at 10 K were made at the BT-1 beamline of the NIST Center for Neutron Research, using two different monochromators: Cu(311) with $\lambda = 1.5403$ Å and Ge(733) with $\lambda = 1.1968$ Å. The use of two wavelengths helped to decouple site occupancies from thermal factors. The Cu(311) monochromator has higher intensity and achieves good resolution at mid-range scattering angles, whereas the Ge(733) has less than one-third of the intensity of Cu(311), but achieves better resolution at high scattering angles. Combined double-wavelength Rietveld refinements took full advantage of these data (Table 3). All samples were refined in the $I4/mmm$ space group using the following atomic positions: R (rare earth), $4e[0\ 0\ z]$; Cu, $2a[0\ 0\ 0]$; O(1), $4c[0\ 1/2\ 0]$; O(2), $4d[0\ 1/2\ 1/4]$. The occupancies were normalized to yield a Pr + Ce occupancy of one. On the rare-earth site, only the occupancy of La was refined, because Pr and Ce have very similar neutron scattering lengths. The occupancy of O(2) was also fixed to its ideal value. The Cu bond valences were calculated[26] using the site occupancies and bond-lengths of each refined structure. The impurity peaks are too weak to observe in neutron powder-diffraction patterns because the rare-earth elements have much smaller neutron-scattering amplitudes relative to Cu and O than was the case for X-rays.

TGA oxygen-loss measurements of an ag-NSC crystal were made while annealing the samples between 24 °C and 830 °C at a vacuum pressure of 5×10^{-5} mbar. Assuming $R_2Cu_{1-f}O_{4-\alpha}$ and $R_2CuO_{4-\beta}$ (R = Pr, La, and Ce) before and after the reduction step respectively, we find $-\alpha + \beta + f(1-\beta) = 0.041$ using Table 3, consistent with TGA measurement of the oxygen loss of 0.04. The consideration of small rare-earth deficiencies does not influence the conclusions.

References

1. Bednorz, J. G. & Müller, K. A. Possible High T_c Superconductivity in the Ba–La–Cu–O System. *Z. Phys. B* **64**, 189–193 (1986).
2. Tokura, Y., Takagi, H. & Uchida, S. A superconducting copper oxide compound with electrons as the charge carriers. *Nature* **337**, 345–347 (1989).
3. Takagi, H., Uchida, S. & Tokura, Y. Superconductivity produced by electron doping in CuO_2-layered compounds. *Phys. Rev. Lett.* **62**, 1197–1200 (1989).
4. Takayama-Muromachi, E., Izumi, F., Uchida, Y., Kato, K. & Asano, H. Oxygen deficiency in the electron-doped superconductor $Nd_{2-x}Ce_xCuO_{4-y}$. *Physica C* **159**, 634–638 (1989).
5. Cava, R. J. *et al.* Metal atom stoichiometry in the electron doped superconductor $(Nd, Ce)_2CuO_4$. *Physica C* **199**, 65–72 (1992).
6. Kim, J. S. & Gaskell, D. R. The phase stability diagrams for the systems $Nd_2CuO_{4-\delta}$ and $Nd_{1.85}Ce_{0.15}O_{4-\delta}$. *Physica C* **209**, 381–388 (1993).
7. Jiang, W., Peng, J. L., Li, Z. Y. & Greene, R. L. Transport properties of $Nd_{1.85}Ce_{0.15}O_{4\pm\delta}$ crystals before and after reduction. *Phys. Rev. B* **47**, 8151–8155 (1993).
8. Radaelli, P. G., Jorgensen, J. D., Schultz, A. J., Peng, J. L. & Greene, R. L. Evidence of apical oxygen in Nd_2CuO_y determined by single-crystal neutron diffraction. *Phys. Rev. B* **49**, 15322–15326 (1994).
9. Prado, F., Caneiro, A. & Serquis, A. Oxygen non-stoichiometry of $Nd_{1.85}Ce_{0.15}Cu_{1+x}O_y$ as a function of δ and its relation with the superconducting properties. *J. Therm. Anal.* **48**, 1027–1038 (1997).
10. Xu, X. Q., Mao, S. N., Jiang, W., Peng, J. L. & Greene, R. L. Oxygen dependence of the transport properties of $Nd_{1.78}Ce_{0.22}CuO_{4\pm\delta}$. *Phys. Rev. B* **53**, 871–875 (1996).
11. Schultz, A. J., Jorgensen, J. D., Peng, J. L. & Greene, R. L. Single-crystal neutron-diffraction structures of reduced and oxygenated $Nd_{2-x}Ce_xCuO_y$. *Phys. Rev. B* **53**, 5157–5159 (1996).
12. Seffar, A. *et al.* Copper deficiency and superconductivity in $Nd_{2-x}Ce_xCuO_4$ oxides. *Physica C* **259**, 75–82 (1996).
13. Prado, F., Briático, J., Caneiro, A., Tovar, M. & Causa, M. T. Copper Content and Superconductivity of $Nd_{1.85}Ce_{0.15}Cu_{1+x}O_y$. *Solid State Commun.* **90**, 695–699 (1994).
14. Uefuji, T., Kurahashi, K., Fujita, M., Matsuda, M. & Yamada, K. Electron-doping effect on magnetic order and superconductivity in $Nd_{2-x}Ce_xCuO_4$ single crystals. *Physica C* **378–381**, 273–277 (2002).
15. Kurahashi, K., Matsushita, H., Fujita, M. & Yamada, K. Heat treatment effects on the superconductivity and crystal structure of $Nd_{1.85}Ce_{0.15}CuO_4$ studied using a single crystal. *J. Phys. Soc. Jpn.* **71**, 910–915 (2002).
16. Richard, P. *et al.* Role of oxygen nonstoichiometry and the reduction process on the local structure of $Nd_{2-x}Ce_xCuO_{4\pm\delta}$. *Phys. Rev. B* **70**, 064513 (2004).
17. Riou, G., Richard, P., Jandl, S., Poirier, M. & Fournier, P. Pr^{3+} crystal-field excitation study of apical oxygen and reduction processes in $Pr_{2-x}Ce_xCuO_{4\pm\delta}$. *Phys. Rev. B* **69**, 024511 (2004).
18. Matsuura, M. *et al.* Effect of a magnetic field on the long-range magnetic order in insulating Nd_2CuO_4 and nonsuperconducting and superconducting $Nd_{1.85}Ce_{0.15}CuO_4$. *Phys. Rev. B* **68**, 144503 (2003).
19. Mang, P. K. *et al.* Phase decomposition and chemical inhomogeneity in $Nd_{2-x}Ce_xCuO_{4\pm\delta}$. *Phys. Rev. B* **70**, 094507 (2004).
20. Kang, H. J. *et al.* Electronically competing phases and their magnetic field dependence in electron-doped nonsuperconducting and superconducting $Pr_{0.88}LaCe_{0.12}CuO_{4\pm\delta}$. *Phys. Rev. B* **71**, 214512 (2005).
21. Kimura, H. *et al.* X-ray and electron diffraction study of a precipitation phase in $Nd_{1.85}Ce_{0.15}CuO_{4+y}$ single crystal. *J. Phys. Soc. Jpn.* **74**, 2282–2286 (2005).
22. Richard, P., Poirier, M., Jandl, S. & Fourier, P. Impact of the reduction process on the long-range antiferromagnetism in $Nd_{1.85}Ce_{0.15}CuO_4$. *Phys. Rev. B* **72**, 184514 (2005).
23. Higgins, J. S., Dagan, Y., Barr, M. C., Weaver, B. D. & Greene, R. L. Role of oxygen in the electron-doped superconducting cuprates. *Phys. Rev. B* **73**, 104510 (2006).
24. Tsuei, C. C. & Kirtley, J. R. Pairing symmetry in cuprate superconductors. *Rev. Mod. Phys.* **72**, 969–1016 (2000).
25. Shan, L. *et al.* Distinct pairing symmetries in $Nd_{1.85}Ce_{0.15}CuO_{4-y}$ and $La_{1.89}Sr_{0.11}CuO_4$ single crystals: evidence from comparative tunneling measurements. *Phys. Rev. B* **72**, 144506 (2005).
26. Brese, N. E. & O'Keeffe, M. Bond-valence parameters for solids. *Acta Cryst. B* **47**, 192–197 (1991).
27. Dai, P. *et al.* Electronic inhomogeneity and competing phases in electron-doped superconducting $Pr_{0.88}LaCe_{0.12}CuO_{4-\delta}$. *Phys. Rev. B* **71**, 100502(R) (2005).
28. Wilson, S. D. *et al.* Resonance in the electron-doped high-transition-temperature superconductor $Pr_{0.88}LaCe_{0.12}CuO_{4-\delta}$. *Nature* **442**, 59–62 (2006).
29. Gauthier, J. *et al.* Different roles of cerium substitution and oxygen reduction in transport in $Pr_{2-x}Ce_xCuO_4$ thin films. *Phys. Rev. B* **75**, 024424 (2007).
30. Armitage, N. P. *et al.* Doping dependence of an *n*-type cuprate superconductor investigated by angle-resolved photoemission spectroscopy. *Phys. Rev. Lett.* **88**, 257001 (2002).
31. Matsui, H. *et al.* Direct observation of a nonmonotonic $d_{x^2-y^2}$-wave superconducting gap in the electron-doped high-T_c superconductor $Pr_{0.89}LaCe_{0.11}CuO_4$. *Phys. Rev. Lett.* **95**, 017003 (2005).
32. Smith, M. G., Mathiram, A., Zhou, J., Goodenough, J. B. & Markert, J. T. Electron-doped superconductivity at 40 K in the infinite-layer compound $Sr_{1-y}Nd_yCuO_2$. *Nature* **351**, 549–551 (1991).
33. Kirimoto, S., Ueda, K., Naito, M. & Imai, T. Superconducting thin films of electron-doped infinite-layer $Sr_{1-x}La_xCuO_2$ grown by molecular beam expitaxy. *Physica C* **378–381**, 127–130 (2002).
34. Jung, C. U. *et al.* Synthesis and pinning properties of the infinite-layer superconductor $Sr_{0.9}La_{0.1}CuO_2$. *Physica C* **366**, 299–305 (2002).

Author contributions

P.D., H.J.K., B.J.C. and S.R. designed the experiment. H.J.K., P.D., B.J.C., P.J.C., S.R. and P.L.L. carried out X-ray-scattering experiments. H.J.K. and Q.H. carried out neutron measurements and refinements. H.J.K. carried out ICP measurements. S.L. prepared ceramic and single crystals of PLCCO and carried out TGA measurements. S.K. and Y.A. also grew single crystals of PLCCO. The paper was written by P.D., H.J.K. and B.J.C., and other co-authors made comments on the paper.

Competing financial interests

The authors declare that they have no competing financial interests.